Fractional charge and emergent mass hierarchy in diagonal two-leg t–J cylinders

Yi-Fan Jiang, Hong-Chen Jiang, Hong Yao, and Steven A. Kivelson

Phys. Rev. B **95**, 245105 — Published 6 June 2017

DOI: 10.1103/PhysRevB.95.245105

Fractional charge and emergent mass hierarchy in diagonal two-leg t-J cylinders

Yi-Fan Jiang,[1,2] Hong-Chen Jiang,[3] Hong Yao,[1,4] and Steven A. Kivelson[2]

[1] *Institute for Advanced Study, Tsinghua University, Beijing 100084, China*
[2] *Department of Physics, Stanford University, Stanford, California 94305, USA*
[3] *Stanford Institute for Materials and Energy Sciences, SLAC National Accelerator Laboratory and Stanford University, Menlo Park, CA 94025, USA*
[4] *Collaborative Innovation Center of Quantum Matter, Beijing 100084, China*

(Dated: May 17, 2017)

We define a class of "diagonal" t-J ladders rotated by $\pi/4$ relative to the canonical lattice directions of the square lattice, and study it using density matrix renormalization group (DMRG). Here, we focus on the two-leg cylinder with a doped hole concentration near $x = 1/4$. At exactly $x = 1/4$, the system forms a period 4 charge density wave (CDW) and exhibits spin-charge separation. Slightly away from 1/4 doping we observe several topologically distinct types of solitons with well defined fractionalized quantum numbers. Remarkably, given the absence of any obvious small parameter, the effective masses of the emergent solitons differ by several orders of magnitude.

I. INTRODUCTION

As a paradigm for the description of high temperature superconductors, the t-J model[1], and the closely related Hubbard model[2,3] have been studied extensively by many different numerical methods and are thought to possess a rich phase diagram[4–56]. In most of these studies, the system is taken to be oriented parallel to the primitive lattice vectors of the square lattice. However, in attempting to extrapolate the results to the thermodynamic limit in 2D, it is also useful to study ladders with different geometries[6–9].

A diagonal cylinder, rotated by $\pi/4$ relative to the primitive lattice directions of the sort shown in Fig. 1(a), has several advantages over the usual one. For example, since a mirror symmetry along the unit cell diagonal is preserved, it is possible to make sharp distinctions between states whose signatures on a regular ladder would be identical – for instance, one can distinguish d-wave superconductivity[10–18] from s-wave superconductivity and vertical "stripe" (unidirectional CDW) order[19–31] from "checkerboard" (bidirectional CDW) order, and a nematic phase[32–35] would correspond to a phase that spontaneously breaks this mirror symmetry. Moreover, while on usual ladders of width larger than 2-legs, there is a clear tendency for stripe order to come at the expense of long-range superconducting coherence,

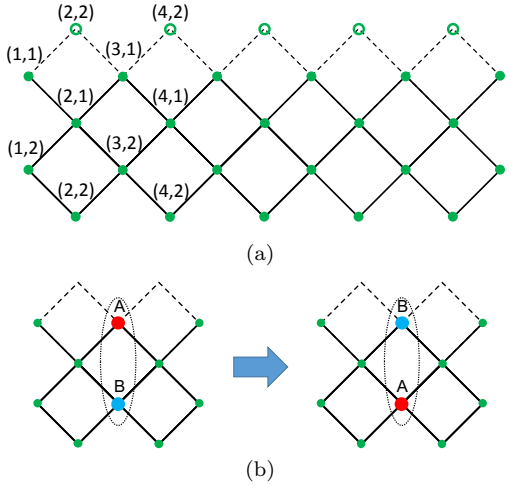

FIG. 1. (a) Diagonal two-leg ladder with cylinder boundary condition (CBC): open in x, periodic in y; empty circles and dashed lines represent the periodic boundary. (b) The local site-exchange symmetry of two leg ladder. The dotted circle indicates one rung. Exchanging the two sites on the rung preserves the Hamiltonian.

Soliton	Spin	Charge	Creation Energy	Dynamical mass
$S_0^{1/2}$	1/2	0	$\lesssim 10^{-4}t$	$\sim 10^{1}t^{-1}$
$S_{\pm e/2}^{0}$	0	$\pm e/2$	$0.206t$	very large
$S_{\pm e}^{0}$	0	$\pm e$	$0.227t$	very large

TABLE I. Physical quantities of three kinds of solitons. The solitons are illustrated in Fig. 4. For charged solitons, their creation energies refer to half of the energy cost of creating a pair of solitons with opposite charge. The dynamical mass is related to the zero-point energy to confine a soliton to a region of size L according to $E \sim \frac{1}{2M^*}(\frac{\pi}{L})^2$.

on diagonal cylinders of appropriate width, CDW order resembling the stripes on a barber pole can involve infinite length stripes, which might therefore compete less strongly with superconducting coherence.

Here we present the first results of a planned extensive DMRG[57,58] study of the t-J model on diagonal ladders with cylinder boundary condition. Although our principle interest in this model concerns the extrapolation to 2D, it is also of interest in the context of multi-component 1D systems. Indeed, the results concerning the 2-leg cylinder near $x = 1/4$ doping are already interesting from this 1D perspective.

At precisely $x = 1/4$, the system exhibits an interesting commensurate CDW with long-range order. While the period of the density wave order is 4 lattice constants, the period 2 "harmonic" is highly dominant and

the period 4 "fundamental" is extremely weak. Looking at the excitation spectrum, in contrast to the usual 2-leg ladder, this diagonal ladder exhibits clear spin-charge separation. Indeed, multiple types of fractionalized soliton excitations arise with different topological characters and associated with different (fractional) quantum numbers, as presented in Table I. These solitons are somewhat analogous to the solitons that arise in the mean-field solution of the electron-phonon (commensurate Peierls) problem[59–61], but here they arise directly from the strong electronic correlations. In particular, we identify two flavors of solitons – one is a highly-local charge excitation with a large creation energy, while the other is an extended spin excitation (spinon) with a creation energy that is at least several orders smaller.

II. MODEL

The Hamiltonian we study in this paper is the nearest neighbor t-J model:

$$H = -t \sum_{\langle ij\rangle\sigma} (c^\dagger_{i\sigma} c_{,j\sigma} + h.c.) + J \sum_{\langle ij\rangle} (\mathbf{S}_i \cdot \mathbf{S}_j - \frac{1}{4} n_i n_j), \quad (1)$$

where $t > 0$ is the uniform hopping integral, $J > 0$ is the superexchange coupling, $c_{i\sigma}$ is the electron annihilation operator at site $i = (x, y)$ with spin polarization $\sigma = \uparrow/\downarrow$, $\mathbf{S}$ is the spin operator, $n_i = \sum_\sigma c^\dagger_{i\sigma} c_{i\sigma}$ is the electron density, and $\langle ij\rangle$ denotes pairs of nearest neighbor sites. We henceforth take units of energy such that $t = 1$. The Hilbert space has a no-double-occupancy constraint, i.e. $n_i = 0, 1$. The lattice structure of the diagonal two-leg cylinder is illustrated schematically in Fig. 1(a). For convenience, we label each site by its location (x, y), where y ranges from 1 to 2 designating the legs and x from 1 to L denoting the position of rungs. In our DMRG simulations of this model, we keep up to 3000 states in the DMRG block and sweep around 30 times such that the truncation error ϵ_{trun} is at most 10^{-7}.

Note that, besides the global symmetries such as the mirror symmetry along diagonal bonds, the Hamiltonian on the diagonal two-leg cylinder exhibits a local symmetry: exchanging the two sites on any rung preserves the Hamiltonian, as illustrated in Fig. 1(b). Since this local site-exchange symmetry on any rung is equivalent to a Z_2 gauge symmetry, the ground states cannot spontaneously break this symmetry due to the Elitzur's theorem[62]. Thus, $\langle \hat{n}_{x,1}\rangle = \langle \hat{n}_{x,2}\rangle$ and $\langle \hat{c}^\dagger_{x,1} \hat{c}_{x',1}\rangle = \langle \hat{c}^\dagger_{x,2} \hat{c}_{x',2}\rangle = \langle \hat{c}^\dagger_{x,1} \hat{c}_{x',2}\rangle = \langle \hat{c}^\dagger_{x,2} \hat{c}_{x',1}\rangle$ for $x \neq x'$. Among other things, this precludes the existence of a nematic phase; this peculiar local symmetry is not a general feature of wider diagonal ladders or cylinders.

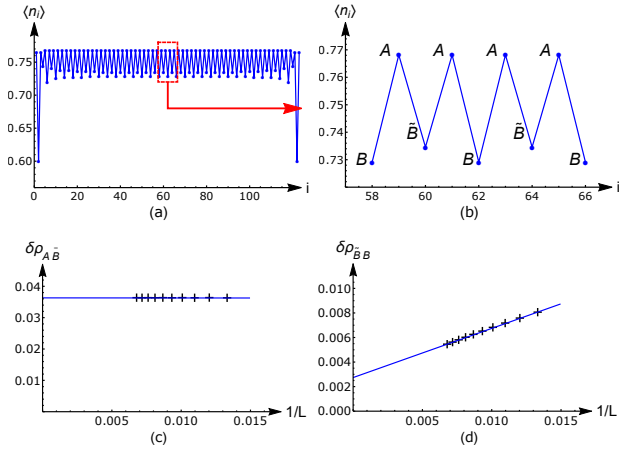

FIG. 2. (a) Density profile of the ground state of a 2×123 diagonal cylinder with 2×31 doped holes. We use an odd length cylinder to minimize the boundary effects. (b) Enlarged view of the red rectangle part in (a). There is a period 4 density pattern $AB\tilde{A}\tilde{B}$. (c) The length dependence of $\delta\rho_{A\tilde{B}} \equiv \rho(A) - [\rho(B) + \rho(\tilde{B})]/2$; extrapolated to the limit $L \to \infty$ this difference approaches $3.631(3) \times 10^{-2}$. (d) The length dependence of $\delta\rho_{\tilde{B}B} \equiv \rho(\tilde{B}) - \rho(B)$; extrapolated to the limit $L \to \infty$ this difference approaches $0.279(3) \times 10^{-2}$. Here ρ is the averaged density of one type of site in the bulk. The lattice length varies from $L = 67$ to 123.

III. DMRG RESULTS AT $x = 1/4$

As usual, the doping level of the system away from the half-filling is defined as $x = 1 - \frac{1}{N}\sum_{i\sigma}\langle c^\dagger_{i\sigma} c_{i\sigma}\rangle$, where $N = 2L$ is total number of sites. We perform large-scale DMRG simulations to study the t-J model on the diagonal two-leg cylinder with open boundary conditions along the leg direction, we adopt a canonical value of $J/t = 1/3$, and for present purposes we focus on the doping around $x = 1/4$. Since all correlation functions on the legs are exactly same we show numerical results only on the leg $y = 1$.

It turns out that the diagonal cylinder at finite doping has many delicate metastable states as shown previously[6] such that its ground states and low energy excitations have not previously been obtained. In order to sort out the lowest energy states by DMRG simulation, we employ the strategy of applying appropriate training fields during the calculations whose details are discussed in the Appendix A.

The ground-state charge density profile of a 2×123 cylinder with 2×31 holes is shown in Fig. 2(a). Although the average value of x differs slightly from 1/4, deep in the bulk (*i.e.* far from the open boundary) $x = 1/4$, as discussed below. We find that the ground state of the system exhibits commensurate period 4 CDW, with a periodic pattern of sites of the form $AB\tilde{A}\tilde{B}$, as clearly shown in the zoomed in region in Fig. 2(b). The difference in the density on the A and the average of the B and $\tilde{B}$ type sites, $\delta\rho_{A\tilde{B}} \equiv \rho(A) - [\rho(B) + \rho(\tilde{B})]/2$, is

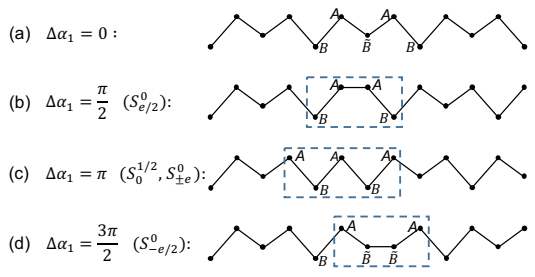

FIG. 3. Schematic illustrations of three topologically distinct domain walls. The first chain is a reference without any domain walls. The three dashed rectangles below enclose the domain walls with different subtended angle $\Delta\alpha_1$. Each domain wall is associated with different solitons S.

an order of magnitude larger than the difference between the B and $\tilde{B}$ type sites, $\delta\rho_{\tilde{B}B} \equiv \rho(\tilde{B}) - \rho(B)$. To understand the significance of this, note that in the limit $\delta\rho_{\tilde{B}B} \to 0$, the CDW would have period 2; in Fourier transform, this means the "fundamental" period 4 mode has a small amplitude $\sim \delta\rho_{\tilde{B}B}$ while the period 2 first harmonic has a large magnitude $\sim \delta\rho_{A\tilde{B}}$. To obtain a quantitative estimate valid in the thermodynamic limit, we compute $\delta\rho_{A\tilde{B}}$ and $\delta\rho_{\tilde{B}B}$ for $L = 8n + 3$ with various n and then plot the results as a function of $1/L$. Here we choose system length $L = 8n + 3$ to minimize the boundary effects. The same result can be obtained in the bulk of cylinders of any L. As shown in Fig. 2(c) and (d), both density differences vary linearly with $1/L$ and approach finite values in the thermodynamic limit: $\delta\rho_{A\tilde{B}} \to 3.631(3) \times 10^{-2}$ and $\delta\rho_{\tilde{B}B} \to 2.79(3) \times 10^{-3}$.

The ground-state always lies in the spin 0 sector. However, although, as we discuss below, there are theoretical reasons to expect a spin-gap, if such a gap exists it is exceedingly small.

A. Solitons in the LG effective field theory

As it is an aid to intuition, we can express the CDW in terms of the ground-state configuration of a pair of complex scalar fields, $\phi_1 \equiv |\phi_1|e^{i\alpha_1}$ and $\phi_2 \equiv |\phi_2|e^{i\alpha_2}$, representing the two harmonics of the density wave:

$$\rho(x) = \bar{\rho} + |\phi_1| \sin\left(\frac{\pi}{2}x + \alpha_1\right) + |\phi_2| \cos\left(\pi x + \alpha_2\right) \quad (2)$$

where $\bar{\rho} = \frac{3}{4}$ is the average density, and the four symmetry related ground-states correspond to $|\phi_1| = \frac{1}{2}\delta\rho_{\tilde{B}B} \ll |\phi_2| = \frac{1}{2}\delta\rho_{A\tilde{B}}$, $\alpha_2 = 2\alpha_1$, and $\alpha_1 = n\pi/2$ with $n = 0$, 1, 2, and 3. In terms of these fields, we could write an effective Landau-Ginzburg Lagrangian of the form

$$\mathcal{L}[\phi_1, \phi_2] = \mathcal{L}_1[\phi_1] + \mathcal{L}_2[\phi_2] - \frac{\lambda_1}{4}\left[(\phi_1)^4 + c.c.\right] \quad (3)$$
$$-\frac{\lambda_2}{2}\left[(\phi_2)^2 + c.c.\right] - \lambda_{12}\left[\phi_2^*(\phi_1)^2 + c.c.\right] + \ldots$$

where $\mathcal{L}_j$ are of the usual form as for an incommensurate CDW, and the terms proportional to λ_j produce the commensurate lock-in to the lattice. The term proportional to λ_{12} locks the relative phase of the two harmonics, and since it is linear in ϕ_2, its presence implies that in any state with non-zero ϕ_1 there will necessarily be an induced (possibly small) harmonic, ϕ_2. The only really unusual feature here is that the parameters which enter $\mathcal{L}_j$ are such that the ground-state magnitude of ϕ_2 is, in fact, much larger than ϕ_1.

Topological solitons (domain walls) with fractional quantum number appear as low energy excitations in Peierls systems[59–61]. Analogously, we find stable topological solitons which carry different (fractional) quantum numbers. Specifically, we expect 3 distinct domain walls which can be characterized by the phase change $\Delta\alpha_1$ (subject to the constraint $\Delta\alpha_2 = 2\Delta\alpha_1$), as shown in Fig. 3. From a topological perspective, the $\Delta\alpha_1 = \pi$ and $3\pi/2$ domain walls can be viewed as bound-states of, respectively, two and three $\Delta\alpha_1 = \pi/2$ domain walls.

B. Solitons from DMRG

We induce soliton states by adding holes or electrons, by flipping spins, or by applying (and then removing) suitable training fields.

(1) The ground state density and spin profile in the sector of $S^z_{tot} = 1$ are shown in Fig. 4(a). The changes relative to the ground-state are spread out. However, it is apparent that the spin-density is doubly peaked, with spin 1/2 in each half of the system, consistent with the existence of two delocalized spin 1/2 particles. Manifestly, these particles are neutral. Moreover, comparing CDW pattern in the middle and at the boundaries of the cylinder, we find a π phase shift. We conclude that the spin 1 ground-state consists of two delocalized neutral spin-$\frac{1}{2}$ solitons with $\Delta\alpha_1 = \pi$, which we label as $S^{1/2}_0$ in Fig. 3(c). The soliton creation energy, $\Delta^{s=1/2}_{c=0}$, is expected to approach half of the spin gap, Δ_s in the limit $L \to \infty$. As we will see, Δ_s is sufficiently small, $\Delta_s \lesssim 10^{-4}$, that we cannot determine its $L \to \infty$ value from even the largest system sizes we have studied. The dynamical mass M^* refers to the zero-point energy to confine a soliton to a region of size L according to $E \sim \frac{1}{2M^*}(\frac{\pi}{L})^2$. As explained in the Appendix B, we extract the dynamical mass of spin-$\frac{1}{2}$ soliton $M^*_s \sim 10^1$ in the small L region.

(2) A metastable excited state with $S^z_{tot} = 0$ can be prepared by applying a proper training field in the initial DMRG simulation, with the result shown in Fig. 4(b). It contains charge $\pm e$ and spin-0 solitons ($S^0_{\pm e}$) with $\Delta\alpha_1 = \pi$. The solitons are sufficiently "heavy" that they remain localized for as many DMRG iterations as we can execute, which also means the dynamical mass of charged solitons M^*_e is effectively infinity. The creation energy of a pair of charge $\pm e$ solitons is $\Delta^{s=0}_{c=e} + \Delta^{s=0}_{c=-e} = 0.453$, which is much larger than $\Delta^{s=1/2}_{c=0}$. Note there is no particle-hole

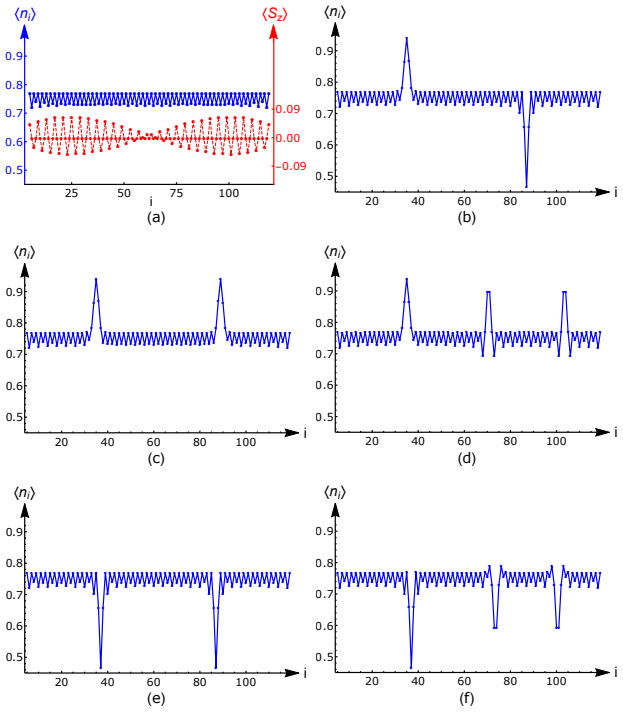

FIG. 4. Density profiles of the $L = 123$ lattice with $5 \leq i \leq 118$ (excluding boundary regions). (a) The ground state with 2×31 doped holes and $S_z^{tot} = 1$ supports two neutral solitons. The density and spin are shown in blue and red respectively. (b) A metastable state with $S_z^{tot} = 0$ and 2×31 doped holes. (c-d) Two metastable states with $S_z^{tot} = 0$ and 2×30 doped holes. (e-f) Two metastable states with $S_z^{tot} = 0$ and 2×32 doped holes.

symmetry relating the solitons with opposite charge.

(3) The addition of two electrons with $S^z_{tot} = 0$ to the "undoped" system (with $x = 1/4$) results in various configurations, depending on the form of the initial training fields. In Fig. 4(c), two S^0_e solitons identical to the left soliton in Fig. 4(b) are clearly seen. In Fig. 4(d), the right soliton has been broken into two $S^0_{e/2}$ solitons, each associated with a $\Delta\alpha_1 = \pi/2$ domain wall (Fig. 3(d)). By comparing the energies of the states in Fig. 4(c) and Fig. 4(d), we obtain $2\Delta^{s=0}_{c=e/2} - \Delta^{s=0}_{c=e} = 0.021$. Similarly, by adding two holes we can obtain the soliton configurations shown in Fig. 4(e) and Fig. 4(f). In Fig. 4(f), there are two charge $-e/2$ solitons associated with the $\Delta\alpha_1 = 3\pi/2$ domain walls. By comparing energies in Fig. 4(e) and Fig. 4(f), we obtain $2\Delta^{s=0}_{c=-e/2} - \Delta^{s=0}_{c=-e} = 0.350$. A charge $-e$ soliton has much lower creation energy than a pair of $-e/2$ solitons, which means that the binding between two charge $-e/2$ solitons can be induced. However, comparing with the dynamical mass, this binding energy is very tiny. As discussed before, due to this large dynamical mass, the charged solitons remain localized in simulations. Therefore, we can observe both integer charges and fractional charges in DMRG simulations.

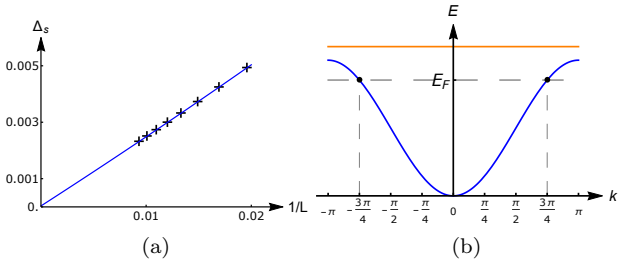

FIG. 5. (a) Dependence of the spin gap on $1/L$; the extrapolation $L \to \infty$ yields $\Delta_s = 3.0(1) \times 10^{-5}$. L varies from 51 to 99. (b) The schematic band dispersion of diagonal two-leg cylinder at one quarter doping. The orange line is the unoccupied flat band. The blue one is the dispersive band with two Fermi points (black dots) at $k_F = \pm 3\pi/4$.

IV. SPINON EXCITATION

As mentioned above, the spin gap at $x = 1/4$ doping is extremely small, which is a novel feature worth further understanding. Because of the period 4 CDW ordering, the enlarged unit cell now has 8 sites and consequently 6 electrons. Thus, consistent with Haldane's conjecture, we should expect a finite spin gap. For finite L, Δ_s is always larger than 0, but by extrapolation we would infer that $\Delta_s \to 3.0 \times 10^{-5}$ as $L \to \infty$, as shown in Fig. 5(a). This is a small enough value that it could be consistent with $\Delta_s \to 0$. More importantly, it would imply a spin-correlation length, $\xi_s \sim J/\Delta_s$, which is larger than any accessible system size, making the quantitative aspect of this estimate unreliable. At an intuitive level, the small gap is related to the small value of the principle harmonic of the CDW; in the limit $\delta\rho_{B\tilde{B}} \to 0$, the CDW has period 2 with 3 electrons per unit cell, and hence (presumably) no spin-gap.

To flesh out this intuition, we consider the same problem in the context of a "bosonized" effective field theory. The non-interacting band structure consists of a flat band[63] and a dispersing band, as shown in Fig. 5(b). For $x = 1/4$, the lower dispersive band is partially filled with $k_F = 3\pi/4$, while the flat band is empty. Thus, by adiabatic continuity, we expect that the low energy fermionic modes can be expressed in terms of two bosonic fields ϕ_c, ϕ_s and their duals, θ_c, θ_s:

$$\psi_{\sigma,\lambda}(x) = \mathcal{N}_\sigma e^{i\lambda k_F x} \exp[-i\sqrt{\frac{\pi}{2}}(\theta_c + \sigma\theta_s + \lambda\phi_c + \lambda\sigma\phi_s)],$$

where $\sigma = \pm 1$ is the polarization of the spin and $\lambda = \pm 1$ for right and left moving fermions. The period 2 and 4 CDW orders come from the expectation value of $\mathcal{O}_{4k_F} \equiv \psi^\dagger_{\uparrow,+}\psi^\dagger_{\downarrow,+}\psi_{\downarrow,-}\psi_{\uparrow,-}$ and $\mathcal{O}_{2k_F} \equiv \psi^\dagger_{\sigma,+}\psi_{\sigma,-}$ respectively:

$$\mathcal{O}_{4k_F} = \mathcal{N}_{4k_F} e^{i3\pi x} e^{i\sqrt{8\pi}\phi_c}, \tag{4}$$

$$\mathcal{O}_{2k_F} = \mathcal{N}_{2k_F} e^{i3\pi x/2} e^{i\sqrt{2\pi}\phi_c} \cos[\sqrt{2\pi}\phi_s]. \tag{5}$$

Because of the $\cos[\sqrt{2\pi}\phi_s]$ factor in Eq. (5), ordering of $\mathcal{O}_{2k_F}$, *i.e.* a period 4 CDW, requires condensing ϕ_s,

which gives rise to a finite spin gap Δ_s. To obtain an estimate of the expected gap magnitude, we invoke the expected scaling relations $\langle e^{i\sqrt{8\pi}\phi_c}\rangle \sim [\langle e^{i\sqrt{2\pi}\phi_c}\rangle]^4$ and $\langle\cos[\sqrt{2\pi}\phi_s]\rangle \sim \sqrt{\Delta_s/\Omega}$ where Ω is a UV cutoff to obtain

$$\Delta_s \sim \frac{\langle \mathcal{O}_{2k_F}\rangle^2}{\sqrt{\langle \mathcal{O}_{4k_F}\rangle}}\Omega. \tag{6}$$

By further identifying $\langle \mathcal{O}_{2k_F}\rangle \sim \delta\rho_{\bar{B}B}$, $\langle \mathcal{O}_{4k_F}\rangle \sim \delta\rho_{A\bar{B}}$, and $\Omega \sim t$, we estimate $\Delta_s \sim 4\times 10^{-5}$ which is small and remarkably consistent with the estimate obtained from finite-size scaling.

V. CONCLUDING REMARKS

From both numerical results and bosonization analysis, we infer that the creation energy of the spinon $\Delta_{c=0}^{s=1/2}$ is extremely small. This is a quite surprising result; the creation energies of the charged solitons are three or four orders of magnitude larger. Without any fine tuning or small parameters in the microscopic model, a striking mass hierarchy emerges in the low energy physics of the t-J model on the diagonal two-leg cylinder!

We have also carried out similar DMRG studies for values of J/t other than $1/3$, including $J/t = 1/4, 1/6, 1/10$. We find qualitatively similar results both for the fractional quantum numbers of the solitons at $x = 1/4$ and the mass hierarchy. Therefore, this mass hierarchy occurs without fine tuning close to the quantum critical point[64]. For other values of x, still more complicated forms of solitons arise. A systematic study of the phase diagram as a function of both J/t and x will be discussed in future work.

ACKNOWLEDGMENTS

YFJ and HY were supported in part by the NSFC under Grant No. 11474175 at Tsinghua University. HCJ was supported by the Department of Energy, Office of Science, Basic Energy Sciences, Materials Sciences and Engineering Division, under Contract DE-AC02-76SF00515. SAK was supported in part by NSF grant #DMR 1265593 at Stanford University.

Appendix A: Details of DMRG simulations

Due to the delicate metastable states, the DMRG simulation of diagonal cylinder easily converges at a local minimum. To encounter this problem, we apply a training field in the initial step of DMRG simulation to help it converge to the low energy state. Different from the pining field which is permanently applied to pin down the orders, the training field is removed after few sweeps so it does not introduce additional bias in the simulation. In our model, the simple external training field term in Hamiltonian reads:

$$H_{train} = \sum_{x,y,\sigma} u(x,y) n_{x,y,\sigma}$$
$$u(x,y) = u_0(-1)^x \max(0, \frac{N_0 - n_{sweep}}{N_0}) \ , \tag{A1}$$

here $u_0 \sim 10^0$ is a constant number, and n_{sweep} counts the DMRG sweep. The external potential $u(x,y)$ plays a role as a training field which is gradually reduced during DMRG sweeps. In our calculation, this training term is finally removed after 14 sweeps ($N_0 = 15$).

The initial training field in Eq. (A1) leads to a perfect CDW state which has the lowest energy. More importantly, via H_{train} we can even take advantage of those high energy metastable states to study the property of soliton excitations. By slightly changing the form of $u(x,y)$, we can create different CDW domain walls and study the physics property of soliton excitations associated with them. Here we take the metastable state shown in Fig. 4(b) as an example. To create a pair of charge $\pm e$ solitons at location x_+ and x_- respectively, we can simply change the external training field $u(x_+ \pm \delta, y) \to -|u(x_+ \pm \delta, y)|$ and $u(x_- \pm \delta, y) \to |u(x_- \pm \delta, y)|$, where $\delta = 0, 1, 2$. This training field can make the DMRG simulation stuck at the metastable state with two solitons at the first few sweeps. After the training field is removed, this metastable state remains even after we tried nearly 400 more sweeps. In general, the metastable state will tunnel to the ground state after sufficient times of sweeps and kept states. However, due to the extremely heavy masses of the soliton excitations, this tunneling process hasn't been observed in our simulation up to 6000 kept state and 400 sweeps.

Appendix B: Creation energy and dynamical mass of solitons

We study two types of effective masses of the solitons. One is the creation energy Δ, which in the context of a relativistic quantum field theory is referred to as the mass. The second is the dynamical mass M^*, which determines the extent to which the soliton tends to delocalized - specifically, the energy to localize the soliton in a (large) box of length L is $\frac{1}{2M^*}(\frac{\pi}{L})^2$.

For charged solitons, we can measure their creation energy by creating a pair of solitons with opposite charges. However, their dynamical masses are almost infinite within the present level of computational accuracy because they remain localized even after hundreds of DMRG sweeps.

For spin-1/2 solitons, both their creation energy and dynamical masses are much smaller than the charged ones. We can measure the dynamical mass of the spin solitons by looking at the energy of two soliton states as a function of system size. As an extended excitation, the interaction between the two solitons need be considered.

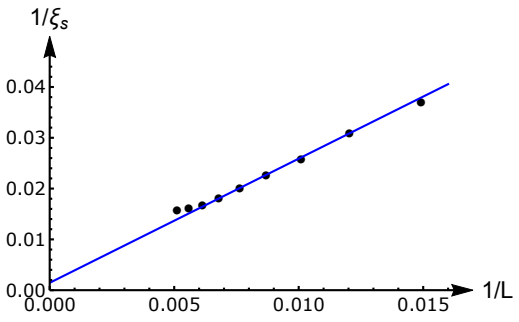

FIG. 6. Length dependence of inverse of spin-spin correlation length $1/\xi_s$ on systems varied from $L = 67$ to 195.

For small enough L, we can write down a perturbative theory in powers of interaction V:

$$\Delta_s(L) = \Delta_s(\infty) + \frac{1}{2M^*}\frac{5\pi^2}{L^2} + \frac{V}{L}\big[A + BL^{-2} + \cdots\big] - V^2 M^* L^{-1}\big[C + \cdots\big] + \cdots \quad \text{(B1)}$$

where $\Delta_s(\infty)$ is the creation energy, $\frac{1}{2M^*}\frac{5\pi^2}{L^2}$ is the energy to localize two non-interacting solitons in a system of length L. A, B and C are constant. The perturbation theory breaks down at large L. By fitting $\Delta_s(L)$ at small L region, we obtain $M^* \approx 28 \sim O(10^1)$.

Appendix C: Spin-spin correlations

On the relatively small systems (comparing with large $\xi_s \sim J/\Delta_s$), we measure the spin-spin correlation function $S(i,j) = \langle \mathbf{S}_{i,1} \cdot \mathbf{S}_{j,1} \rangle \sim e^{-|i-j|/\xi_s}$ in a higher accuracy $\epsilon_{trun} < 10^{-10}$ and find a rather long correlation length ξ_s which is compatible to the system size, as shown in Fig. 6. The blue line stands for the linear fitting of $1/\xi_s$ in the small system sizes. It means that the correlation length ξ_s increases when the cylinder becomes longer, which supports that ξ_s is restricted by the small system sizes. Though the linear fitting indicates that $1/\xi_s$ is close to 0 in the thermodynamic limit, the data from larger system ($L \geq 163$) shows a deviation from blue line which weakly implies a finite correlation length in the thermodynamic limit.

[1] F. C. Zhang and T. M. Rice, Phys. Rev. B **37**, 3759 (1988).
[2] J. Hubbard, Proc. R. Soc. A **276**, 238 (1963).
[3] P.W. Anderson, Science **235**, 1196 (1987).
[4] E. Dagotto, Rev. Mod. Phys. **66**, 763 (1994).
[5] P. A. Lee, N. Nagaosa, and X.-G. Wen, Rev. Mod. Phys. **78**, 17 (2006).
[6] J. P. F. LeBlanc, A. E. Antipov, F. Becca, I. W. Bulik, G. K.-L. Chan, C.-M. Chung, Y. Deng, M. Ferrero, T. M. Henderson, C. A. Jiménez-Hoyos, E. Kozik, X.-W. Liu, A. J. Millis, N. V. Prokof'ev, M. Qin, G. E. Scuseria, H. Shi, B. V. Svistunov, L. F. Tocchio, I. S. Tupitsyn, S. R. White, S. Zhang, B.-X. Zheng, Z. Zhu, and E. Gull (Simons Collaboration on the Many-Electron Problem), Phys. Rev. X **5**, 041041 (2015).
[7] J.-B. Fouet, F. Mila, D. Clarke, H. Youk, O. Tchernyshyov, P. Fendley, and R. M. Noack, Phys. Rev. B **73**, 214405 (2006).
[8] E. Berg, S. A. Kivelson, and D. J. Scalapino, New Journal of Physics **11**, 085007 (2009).
[9] E. Berg, S. A. Kivelson, and D. J. Scalapino, Phys. Rev. B **81**, 172504 (2010).
[10] E. Dagotto and J. Riera, Phys. Rev. Lett. **70**, 682 (1993).
[11] S. Sorella, G. B. Martins, F. Becca, C. Gazza, L. Capriotti, A. Parola, and E. Dagotto, Phys. Rev. Lett. **88**, 117002 (2002).
[12] A. Himeda, T. Kato, and M. Ogata, Phys. Rev. Lett. **88**, 117001 (2002).
[13] M. Ogata and A. Himeda, J. Phys. Soc. Jpn. **72**, 374 (2003).
[14] D. A. Ivanov, Phys. Rev. B **70**, 104503 (2004).
[15] C. T. Shih, T. K. Lee, R. Eder, C.-Y. Mou, and Y. C. Chen, Phys. Rev. Lett. 92, 227002 (2004).
[16] M. Lugas, L. Spanu, F. Becca, and S. Sorella, Phys. Rev. B **74**, 165122 (2006).
[17] L. Spanu, M. Lugas, F. Becca, and S. Sorella, Phys. Rev. B **77**, 024510 (2008).
[18] W.-J. Hu, F. Becca, and S. Sorella, Phys. Rev. B **85**, 081110 (2012).
[19] D. Poilblanc and T. M. Rice, Phys. Rev. B **39**, 9749 (1989).
[20] J. Zaanen and O. Gunnarsson, Phys. Rev. B **40**, 7391 (1989).
[21] K. Machida, Physica (Amsterdam) **158C**, 192 (1989).
[22] H. Schulz, J. Phys. (Paris) **50**, 2833 (1989).
[23] S. R. White and D. J. Scalapino, Phys. Rev. Lett. **80**, 1272 (1998).
[24] S. R. White and D. J. Scalapino, Phys. Rev. B **70**, 220506 (2004).
[25] E. Berg, E. Fradkin, E.-A. Kim, S. A. Kivelson, V. Oganesyan, J. M. Tranquada, and S. C. Zhang, Phys. Rev. Lett. **99**, 127003 (2007).
[26] M. Vojta and O. Rösch, Phys. Rev. B **77**, 094504 (2008).
[27] S. R. White and D. J. Scalapino, Phys. Rev. B **79**, 220504 (2009).
[28] K.-Y. Yang, W. Q. Chen, T. M. Rice, M. Sigrist, and F.-C. Zhang, New J. Phys. **11**, 055053 (2009).
[29] C.-P. Chou and T.-K. Lee, Phys. Rev. B **81**, 060503 (2010).
[30] M. Greiter and H. Schmidt, Phys. Rev. B **83**, 144422 (2011).
[31] D. Scalapino and S. White, Physica (Amsterdam) **481C**, 146 (2012).
[32] F. Becca, L. Capriotti, and S. Sorella, Phys. Rev. Lett. **87**, 167005 (2001).
[33] B. Normand and A. P. Kampf, Phys. Rev. B **64**, 024521 (2001).
[34] A. P. Kampf, D. J. Scalapino, and S. R. White, Phys. Rev. B **64**, 052509 (2001).
[35] M. Capello, M. Raczkowski, and D. Poilblanc, Phys. Rev. B **77**, 224502 (2008).

[36] W. O. Putikka, M. U. Luchini, and T. M. Rice, Phys. Rev. Lett. **68**, 538 (1992).
[37] R. Valentí and C. Gros, Phys. Rev. Lett. **68**, 2402 (1992).
[38] M. Kohno, Phys. Rev. B **55**, 1435 (1997).
[39] C. T. Shih, Y. C. Chen, and T. K. Lee, Phys. Rev. B **57**, 627 (1998).
[40] M. Calandra, F. Becca, and S. Sorella, Phys. Rev. Lett. **81**, 5185 (1998).
[41] M. Raczkowski, M. Capello, D. Poilblanc, R. Frésard, and A. M. Oleś, Phys. Rev. B **76**, 140505 (2007).
[42] C.-P. Chou, N. Fukushima, and T. K. Lee, Phys. Rev. B **78**, 134530 (2008).
[43] S. R. White and D. J. Scalapino, Phys. Rev. B **61**, 6320 (2000).
[44] L. Liu, H. Yao, E. Berg, S. R. White, and S. A. Kivelson, Phys. Rev. Lett. **108**, 126406 (2012).
[45] Z. Zhu, H.-C. Jiang, D.-N. Sheng, and Z.-Y. Weng, Sci. Rep. **4**, 5419 (2014).
[46] Z. Zhu, C. Tian, H.-C. Jiang, Y. Qi, Z.-Y. Weng, and J. Zaanen, Phys. Rev. B **92**, 035113 (2015).
[47] S. R. White, D. J. Scalapino, and S. A. Kivelson, Phys. Rev. Lett. **115**, 056401 (2015).
[48] S. Liu, H.-C. Jiang, and T. P. Devereaux, arXiv:1606.03762.
[49] J. Dodaro, H.-C. Jiang, and S. A. Kivelson, in preparation.
[50] V. J. Emery, S. A. Kivelson, and H. Q. Lin, Phys. Rev. Lett. **64**, 475 (1990).
[51] M. Ogata, M. U. Luchini, S. Sorella, and F. F. Assaad, Phys. Rev. Lett. **66**, 2388 (1991).
[52] E. Dagotto, J. Riera, and D. Scalapino, Phys. Rev. B **45**, 5744 (1992).
[53] C. S. Hellberg and E. Manousakis, Phys. Rev. Lett. **83**, 132 (1999).
[54] P. Corboz, S. R. White, G. Vidal, and M. Troyer, Phys. Rev. B **84**, 041108 (2011).
[55] Z.-C. Gu, H.-C. Jiang, D. N. Sheng, H. Yao, L. Balents, and X.-G. Wen, Phys. Rev. B **88**, 155112 (2013).
[56] P. Corboz, T. M. Rice and M. Troyer, Phys. Rev. Lett. **113**, 046402 (2014).
[57] S. R. White, Phys. Rev. Lett. **69**, 2863 (1992).
[58] S. R. White, Phys. Rev. B **48**, 10345 (1993).
[59] N. J. Zabusky and M. D. Kruskal, Phys. Rev. Lett. **15**, 240 (1965).
[60] S. C. Zhang, S. Kivelson, and A. S. Goldhaber, Phys. Rev. Lett. **58**, 2134 (1987).
[61] A. J. Heeger, S. Kivelson, J. R. Schrieffer, and W. P. Su, Rev. Mod. Phys. **60**, 781 (1988).
[62] S. Elitzur, Phys. Rev. D **12**, 3978 (1975).
[63] S. Takayoshi, H. Katsura, N. Watanabe, and H. Aoki, Phys. Rev. A **88**, 063613 (2013).
[64] E. H. Lieb, T. D. Schultz, and D. C. Mattis, Ann. Phys. (N. Y.) **16**, 407 (1961).